

Abstract

Few glaciological field data are available on glaciers in the Hindu Kush – Karakoram – Himalaya (HKH) region, and remote sensing data are thus critical for glacier studies in this region. The main objectives of this study are to document, using satellite images, the seasonal changes of surface albedo for two Himalayan glaciers, Chhota Shigri Glacier (Himachal Pradesh, India) and Mera Glacier (Everest region, Nepal), and to reconstruct the annual mass balance of these glaciers based on the albedo data. Albedo is retrieved from MODerate Imaging Spectroradiometer (MODIS) images, and evaluated using ground based measurements. At both sites, we find high coefficients of determination between annual minimum albedo averaged over the glacier (AMAAG) and glacier-wide annual mass balance (B_a) measured with the glaciological method ($R^2 = 0.75$). At Chhota Shigri Glacier, the relation between AMAAG found at the end of the ablation season and B_a suggests that AMAAG can be used as a proxy for the maximum snowline altitude or equilibrium line altitude (ELA) on winter accumulation-type glaciers in the Himalayas. However, for the summer-accumulation type Mera Glacier our approach relied on the hypothesis that ELA information, mostly not accessible from space during the monsoon, was still preserved later thanks to strong winter winds blowing away snow and in turn exposing again the late monsoon surface. AMAAG was subsequently revealed in the post-monsoon period. Reconstructed B_a at Chhota Shigri Glacier agrees with mass balances previously reconstructed using a positive degree-day method. Reconstructed B_a at Mera Glacier is affected by heavy cloud cover during the monsoon, which systematically limited our ability to observe AMAAG at the end of the melting period. In addition, the relation between AMAAG and B_a is constrained over a shorter time period for Mera Glacier (6 years) than for Chhota Shigri Glacier (11 years). Thus the mass balance reconstruction is less robust for Mera Glacier than for Chhota Shigri Glacier. However our method shows promising results and may be used to reconstruct the annual mass balance of glaciers with contrasted seasonal

TCD

8, 3437–3474, 2014

Surface albedo of Himalayan glaciers and links with mass balance

F. Brun et al.

Title Page

Abstract

Introduction

Conclusions

References

Tables

Figures

◀

▶

◀

▶

Back

Close

Full Screen / Esc

Printer-friendly Version

Interactive Discussion



Surface albedo of Himalayan glaciers and links with mass balance

F. Brun et al.

Title Page

Abstract

Introduction

Conclusions

References

Tables

Figures

◀

▶

◀

▶

Back

Close

Full Screen / Esc

Printer-friendly Version

Interactive Discussion



geodetic method allows a region-wide glacier mass balance to be calculated (Gardelle et al., 2013), and has revealed the heterogeneous response of HKH glaciers to climate change (Gardelle et al., 2013; Kääb et al., 2012). However, the geodetic method provides estimates of height and volume change averaged over typical periods of 5 years or more (e.g., Bolch et al., 2011; Kääb et al., 2012; Nuimura et al., 2012; Gardelle et al., 2013), and therefore fails to capture the inter-annual or seasonal variability of glacier mass balance. Furthermore, although this method is accurate over large regions, it is less efficient when applied to a single glacier for which no high resolution topographic data are available (e.g., Vincent et al., 2013).

The equilibrium-line altitude (ELA) and minimum mean bi-hemispherical broadband albedo (referred to hereafter as albedo) of a glacier have the potential to be good proxies of the annual mass balance in some regions (e.g., Dumont et al., 2012; Rabatel et al., 2013; Shea et al., 2013). On temperate glaciers, the average albedo of a whole glacier surface reaches a minimum at the end of the ablation season, when the elevation of the transient snowline elevation reaches a maximum (Rabatel et al., 2005; Dumont et al., 2012). The maximum elevation of the transient snowline is often referred to as a proxy of the ELA (Rabatel et al., 2005). The ELA, and thus the annual minimum albedo averaged on the whole glacier (AMAAG), is strongly correlated with the annual glacier mass balance (B_a ; Dumont et al., 2012). Here we present the first test of this method on two Himalayan glaciers, Chhota Shigri Glacier and Mera Glacier.

The goal of this study is to examine the links between albedo and B_a at two Himalayan glaciers. Specifically, our objectives are to (1) use ground measurements of albedo to evaluate the accuracy of albedo retrievals algorithms for MODerate Imaging Spectroradiometer (MODIS) data, (2) assess the relation between albedo and B_a , (3) characterize the seasonal variability of the albedo; and (4) use albedo records from MODIS to reconstruct the mass balance of both glaciers since 2000.

2 Sites description and climatic setting

2.1 Chhota Shigri Glacier

Chhota Shigri Glacier (32.3° N, 77.6° E) is a valley-type glacier located in the Chandra-Bhaga River basin, Pir Panjal Range, India (Fig. 1). This glacier extends from 6263 to 4050 m a.s.l. and covers a total area of 15.7 km². It is mostly free of debris except in the lower ablation area (≤ 4500 m a.s.l.). Approximately 3.4 % of the total glacierized area is debris-covered (Vincent et al., 2013). A central moraine separates the glacier into two branches below 4800 m a.s.l., and the glacier is fed by numerous tributaries exhibiting various aspects (Fig. 2). Its glacier-wide annual mass balance has been monitored since 2002 using the ground-based glaciological method (Azam et al., 2012, 2014b). The equilibrium-line altitude for a zero annual mass balance (ELA₀) was found to be close to 4900 m a.s.l. (Wagnon et al., 2007).

2.2 Mera Glacier

Mera Glacier (27.7° N, 86.9° E) is a 5.1 km² debris free glacier situated in the Dudh Koshi basin, Everest region, Nepal (Fig. 1). The main glacier flows from 6420 m a.s.l. and divides into two branches around 5800 m a.s.l. The main branch (referred hereafter as Mera branch, located on the western part of the glacier) flows down to 4940 m a.s.l., while the smaller eastern branch (Naulek branch) flows down to 5260 m a.s.l. The eastern part of the Naulek branch is also part of the Naulek glacierized complex that flows down from Naulek Peak (Fig. 3). Glacier-wide mass balance has been monitored at Mera Glacier since 2007 using the glaciological method, and ELA₀ is close to 5550 m a.s.l. (Wagnon et al., 2013).

2.3 Climate setting

The southern flank of the Himalayas is dominated by two contrasting climate regimes: the westerlies and the Indian summer monsoon. The influence of the Indian monsoon

TCD

8, 3437–3474, 2014

Surface albedo of Himalayan glaciers and links with mass balance

F. Brun et al.

Title Page

Abstract

Introduction

Conclusions

References

Tables

Figures

◀

▶

◀

▶

Back

Close

Full Screen / Esc

Printer-friendly Version

Interactive Discussion



Surface albedo of Himalayan glaciers and links with mass balance

F. Brun et al.

Title Page

Abstract

Introduction

Conclusions

References

Tables

Figures

◀

▶

◀

▶

Back

Close

Full Screen / Esc

Printer-friendly Version

Interactive Discussion



decreases from east to west and dominates the climatic signal for longitudes eastern from approximately 77° E. Conversely, the influence of the westerlies decreases from west to east (Bookhagen and Burbank, 2006, 2010; Yao et al., 2012; Maussion et al., 2013). Monsoon precipitation occurs from June to September as moist air masses from the Bay of Bengal sweep toward the Himalayas. These orographic rainfalls are highly related to the local relief (Bookhagen and Burbank, 2006), with a strong south-north gradient due to the presence of the Himalayan range. At high altitudes, monsoon-season precipitation is characterized by high frequency and low intensity (Shrestha et al., 2012). Westerly circulation patterns bring precipitation mainly during the winter months (November to April). They are produced by synoptic-scale upper-tropospheric waves amplified by the topography with a capacity to generate heavy snowfalls (Hatwar et al., 2005).

Because of both climatic regimes, the seasonality of rainfall varies greatly with the location in the range (Yao et al., 2012). According to Burbank et al. (2012) and local precipitation measurements (e.g., Wagnon et al., 2013), precipitation amount at Mera Glacier is mostly governed by the Indian monsoon, with 70 to 80% of precipitation occurring during summer time (Wagnon et al., 2013). Chhota Shigri Glacier is influenced by both monsoon and westerly circulation systems, and receives precipitation throughout the year (Azam et al., 2014a, b). These observations are consistent with the glaciological data: Mera Glacier is a summer-accumulation type glacier (Maussion et al., 2013; Wagnon et al., 2013), while Chhota Shigri Glacier is a winter-accumulation type glacier despite being located in the transition zone and influenced by both regimes (Wagnon et al., 2007; Maussion et al., 2013).

3 Data and methods

3.1 Field data

Annual mass balance data, calculated with the glaciological method, are available for Chhota Shigri and Mera glaciers over the periods 2002–2013 (Azam et al., 2014b) and 2007–2013 (Wagnon et al., 2013), respectively. The accuracy of the B_a data (Thibert et al., 2008) was estimated to be ± 0.28 m.w.e. for Mera Glacier and ± 0.40 m.w.e. for Chhota Shigri Glacier (Wagnon et al., 2013; Azam et al., 2012).

The accuracy of the albedo retrieval from satellite data was evaluated using short-wave radiation observations from automatic weather stations (AWSs) installed in the ablation zones of the two glaciers (Figs. 2 and 3) at 4670 and 5360 m a.s.l. for Chhota Shigri and Mera glaciers, respectively. Incident and reflected shortwave radiation (SW_{in} and SW_{out} , respectively) were measured with Kipp & Zonen CM1 sensors ($0.3 \leq \lambda \leq 2.8 \mu\text{m}$) every 30 s and averaged every half-hour. According to the manufacturer the sensors have an intrinsic accuracy of $\pm 3\%$. In turn, the albedo, calculated as the ratio between SW_{out} and SW_{in} , has a compounded accuracy of about 4%. Nevertheless, the local slope, the tilt of the device, and frost deposition on the sensor can increase the uncertainty. At Mera Glacier the AWS collected data from 9 November 2009 to 10 November 2010 and from 27 November 2012 to 16 November 2013. At Chhota Shigri Glacier the AWS collected data from 13 August 2012 to 2 February 2013 and from 8 July 2013 to 3 October 2013 (Fig. 4).

Snow and ice albedo are highly sensitive to cloud cover, which affects the ratio of direct and diffuse radiation (e.g., Warren, 1982; Gardner and Sharp, 2010). Therefore, we filtered the data to retain only those collected in clear-sky conditions to be able to compare them to satellite retrieved albedo. To do so, we calculated the local clear-sky broadband atmospheric transmissivity χ as the ratio between the value defining the upper envelope of measured SW_{in} at ground level and that defining the upper envelope of SW_{in} at the top of the atmosphere (TOA) (Garnier and Ohmura, 1968). We found clear-sky χ equal to 0.99 and 0.85 on Mera and Chhota Shigri glaciers, respectively.

Surface albedo of Himalayan glaciers and links with mass balance

F. Brun et al.

Title Page

Abstract

Introduction

Conclusions

References

Tables

Figures

◀

▶

◀

▶

Back

Close

Full Screen / Esc

Printer-friendly Version

Interactive Discussion



Surface albedo of Himalayan glaciers and links with mass balance

F. Brun et al.

Title Page

Abstract

Introduction

Conclusions

References

Tables

Figures

◀

▶

◀

▶

Back

Close

Full Screen / Esc

Printer-friendly Version

Interactive Discussion



Clear-sky days were selected as the days for which χ was in the range $0.99 \pm 4\%$ for Mera Glacier and $0.85 \pm 10\%$ for Chhota Shigri Glacier at local solar noon. The lower estimated atmospheric transmissivity at Chhota Shigri Glacier is likely due to its lower elevation, its sky-view factor, and the vicinity of important aerosol sources. Snow and ice albedo also depend strongly on the solar zenith angle (Warren, 1982). In order to allow a direct comparison between field and satellite measurements, we averaged the AWS albedo over a two-hour time span centered on the MODIS satellite passing time, which is coincident with a high zenithal angle.

3.2 MODIS snow products

3.2.1 MOD10A1 products

Daily MOD10A1 products (referred hereafter as MOD10), processed and provided by the National Snow and Ice Data Centre, are available at <http://nsidc.org> (Hall et al., 2006). The products provide an estimate of daily blue-sky (BS) albedo, which corresponds to the broadband albedo for the actual direct and diffuse illumination, daily snow cover, and a quality assessment (QA) at 500 m resolution (Klein and Stroeve, 2002).

3.2.2 MCD43 products

MODIS MCD43A3 products provide white-sky spectral albedo (WS albedo, which corresponds to the albedo of the surface illuminated only by diffuse irradiance), black-sky spectral albedo (which corresponds to the albedo of the surface illuminated only by direct irradiance), and broadband albedo (called WS shortwave albedo), for the seven visible and near infrared bands of MODIS at local solar noon. MCD43A3 products are produced at 500 m resolution every 8 days using 16 days of MODIS TERRA and AQUA acquisitions. The separate products MCD43A2 are used to provide quality assessment

such a summer-accumulation type glacier, the satellite images obtained immediately after the monsoon already exhibit snow accumulation at higher elevations, hiding the glacier surface representative of the end of ablation season. To tackle this issue we retained only the 16 pixels corresponding to elevations lower than the ELA_0 (5550 m a.s.l.) (Fig. 3). Moreover, calculating the albedo on a small part of the glacier increases the availability of good quality images, especially when the higher part of the glacier is covered by clouds, while the lower part remains cloud-free, which is often observed in spring.

4 Results

4.1 Evaluation of the albedo retrieval

4.1.1 Comparison with field measurements

We compared the broadband albedo measured under clear sky conditions at the AWSs with the BS albedo retrieved by MODImLab and MOD10 algorithm on the corresponding pixel for both glaciers (Fig. 5). As the MCD43 products provide an albedo averaged over 16 days we did not compare it against instantaneous field measurements. The limited number of albedo samples ($n = 15$ for MODImLab and $n = 32$ for MOD10) and the relatively small variance ($\sigma = 0.04$ for the AWS albedo used to compare with MOD10) on Chhota Shigri Glacier prevented a reliable conclusion about the quality of the albedo retrieval techniques (Fig. 5a). As the MOD10 albedo estimates correspond to snow-covered periods at the Chhota Shigri AWS, the regression is poorly constrained. At Mera Glacier the measurement period is long enough to thoroughly assess the quality of the albedo retrieval (Fig. 5b). The agreement between albedo retrieval from MODImLab and AWS measurements is better than between MOD10 and AWS measurements (RMSE are 0.067 and 0.071, respectively). The mean difference between the AWS measurements and MODImLab retrieval is 0.03 vs. 0.18 for MOD10. Thus the MOD10

Surface albedo of Himalayan glaciers and links with mass balance

F. Brun et al.

Title Page

Abstract

Introduction

Conclusions

References

Tables

Figures



Back

Close

Full Screen / Esc

Printer-friendly Version

Interactive Discussion



albedo retrieval appears to be biased towards lower values at the Mera site. This is in contradiction with other studies that found a bias toward higher values in MOD10 data (e.g., Şorman et al., 2007). In conclusion, MODImLab retrieval seems more reliable than MOD10 for the two studied glaciers.

4.1.2 Comparison of cloud masks

The performances of the cloud masks calculated by MODImLab and that provided by the MOD35 Cloud product (and used in MOD10 products) were compared through a visual inspection of 13 ASTER images with variable cloud coverage (Table 3) covering the Mera Glacier area and corresponding to a total of 13312 and 3328 pixels for the 250 and 500 m resolutions respectively (Fig. 6). MODIS and ASTER images were acquired at the same time (no more than 5 minutes apart), and were compared using four categories, taking the ASTER mask determined by visual inspection as a reference:

- Category 1: cloudy pixel observed on ASTER image and classified as cloudy pixel by the cloud detection algorithm
- Category 2: cloudy pixel classified as cloud-free pixel
- Category 3: cloud-free pixel classified as cloudy pixel
- Category 4: cloud-free pixel classified as cloud-free pixel

Successful identification rates for the MODImLab cloud mask and the MOD35 cloud mask were 78 and 73% respectively. The MODImLab cloud mask detected correctly 96% of cloud-obscured pixels, whereas MOD10 detected only 67% (percentages calculated from the frequencies of categories 1 and 2 on Fig. 6). MODImLab misclassified 46% of the cloud-free pixels whereas MOD10 misclassified only 21% of them (percentages calculated from the frequencies of categories 3 and 4 on Fig. 6). Overall, the MODImLab cloud detection algorithm is more conservative than the MOD35 algorithm, as cloud coverage is overestimated. To avoid unrealistic values of albedo retrieved

Surface albedo of Himalayan glaciers and links with mass balance

F. Brun et al.

Title Page

Abstract

Introduction

Conclusions

References

Tables

Figures

◀

▶

◀

▶

Back

Close

Full Screen / Esc

Printer-friendly Version

Interactive Discussion



from MODIS data, we relied on the MODImLab cloud mask at the cost of reducing the number of available images assumed to be free of clouds.

4.2 Multi-annual trend of the albedo signal

Following Ming et al. (2012) we calculated the 2000–2013 trend in MOD10 albedo for the highest elevation pixels of both glaciers (located at 5191 m a.s.l. for Chhota Shigri Glacier and 6008 m a.s.l. for Mera Glacier). The linear trends are $+0.0013$ and -0.0025 yr^{-1} , respectively (Fig. 7). As MODImLab cloud mask is more conservative than MOD35 cloud mask (i.e. the cloud cover is overestimated by MODImLab), the albedo values obtained with MODImLab are not uniformly distributed along the year, and therefore introduce a sampling bias in the trend calculation. Consequently, we did not use MODImLab to compute a multi-annual trend of the albedo signal.

We also compared the MOD10 albedo averaged over 16 days to MCD43 albedo (produced from 16 days of acquisition). MCD43 quality flags guaranteed only 4 % of high quality retrieval (with full bidirectional reflectance function inversion) on Mera Glacier and 21 % on Chhota Shigri Glacier. Such quality assurance was considered too low to use MCD43 albedo products for trend analysis and for the rest of the study.

4.3 Seasonal variations of albedo

We linearly interpolated between the dates with information the mean albedo values at a daily time step to calculate an average albedo cycle for each glacier (Fig. 8). On Chhota Shigri Glacier, the annual signal of albedo exhibits a marked seasonality with a high albedo during winter time (from November to the end of February) steadily decreasing through spring and summer until reaching a minimum in August. The annual minimum albedo is in turn obtained consistently between late July and mid-September (Fig. 8 and Table 2). In contrast, the cycle observed for the lower part of Mera Glacier exhibits a less pronounced seasonality due in part to cloud cover during the monsoon. The glacier is seldom visible from space during summer time, thus potentially

TCD

8, 3437–3474, 2014

Surface albedo of Himalayan glaciers and links with mass balance

F. Brun et al.

Title Page

Abstract

Introduction

Conclusions

References

Tables

Figures

◀

▶

◀

▶

Back

Close

Full Screen / Esc

Printer-friendly Version

Interactive Discussion



4.5 Mass balance reconstruction, 1999–2013

Using the significant relations obtained between albedo and glacier-wide mass balance, we reconstructed B_a for years with available MODIS images. For each year, the AMAAG was retrieved between July and September on Chhota Shigri Glacier, and between August and June the next year on Mera Glacier. These minima were then inverted to estimate B_a , with the linear regression parameters of mass balance expressed as a function of AMAAG (Fig. 10). This method is referred hereafter as the albedo method.

We calculated the uncertainty associated with these reconstructed values by performing two Monte Carlo simulations. First, we did a simulation to obtain a distribution of the regression parameters assuming that the errors on both mass balance and albedo were normally distributed (Fig. 11). Then, using this distribution, for every albedo minimum, we randomly chose 100 000 slope-intercept couples and calculated the corresponding B_a . We kept the values included between the 5th and 95th percentiles of this distribution to obtain the 90 % confidence intervals for the reconstructed mass balance values.

Both the observed and reconstructed B_a values were averaged over their corresponding period of record to allow comparison with the glacier-wide geodetic mass balance reported in Gardelle et al. (2013) for the period 1999–2011. Although a systematic bias may exist between the geodetic mass balance and B_a obtained with the glaciological method used to calibrate the albedo method (e.g., Zemp et al., 2013), this comparison allows us to check the order of magnitude of our results. The average reconstructed mass balance on Chhota Shigri Glacier was found to be $-0.75 \pm 0.11 \text{ m.w.e. yr}^{-1}$, which is significantly more negative than the value derived from the geodetic method ($-0.37 \pm 0.19 \text{ m.w.e. yr}^{-1}$). Nonetheless, the reconstructed B_a values for the period October 1999–October 2002 are in good agreement with the values reconstructed using a degree-day model (Azam et al., 2014a). For Mera Glacier the reconstructed mass balance is on average positive ($0.55 \pm 1.3 \text{ m.w.e. yr}^{-1}$) as was the geodetic mass

Surface albedo of Himalayan glaciers and links with mass balance

F. Brun et al.

Title Page

Abstract

Introduction

Conclusions

References

Tables

Figures



Back

Close

Full Screen / Esc

Printer-friendly Version

Interactive Discussion



Surface albedo of Himalayan glaciers and links with mass balance

F. Brun et al.

Title Page

Abstract

Introduction

Conclusions

References

Tables

Figures

◀

▶

◀

▶

Back

Close

Full Screen / Esc

Printer-friendly Version

Interactive Discussion



related to changes occurring in the atmosphere or due to a drift in MODIS sensors calibration (e.g., Zhang and Reid, 2010). Nevertheless these trends are consistent with those observed by Ming et al. (2012), at glaciers PT1 and PT4, which are located relatively close to Chhota Shigri and Mera glaciers. Albedo trends at PT1 and PT4, respectively, are $+0.0064$ and -0.0011 yr^{-1} . Albedo trends at Chhota Shigri Glacier and Mera Glacier are $+0.0013$ and -0.0025 yr^{-1} , respectively. These trends are both significant for a confidence level of 85 % with a Student test. Ming et al. (2012) observed only negative albedo trends except for the most western glacier of their study PT1. The positive trend we obtained at Chhota Shigri Glacier, close to PT1, seems to confirm this finding.

Special cloud detection algorithms are required in mountainous and high altitude regions (Hall and Riggs, 2007; Sirguey et al., 2009). In particular, thresholds on the different bands, band ratios, and band combinations need adjustments when applied to different regions. For instance, the relatively low water vapour content of the atmosphere above Mera Glacier (clear sky emissivity of 0.99) yields frequent misclassifications of cloud free pixels as high altitude clouds in MODImLab cloud detection algorithm. Our work suggests that independent tuning of cloud detection algorithms is required, and this requires extensive comparison with other interpreted images, a process that is both time consuming and operator dependent.

5.2 Advantages, drawbacks, and robustness of the albedo method applied in the Himalayas

An attractive application of the albedo method is to reconstruct B_a for periods when surface observations are not available. The mass balance reconstruction is robust for Chhota Shigri Glacier but appeared questionable for Mera Glacier. We suggest two main reasons for this difference.

First, persistent cloud coverage at Mera Glacier does not allow the true AMAAG to be resolved in some years. In order to test this hypothesis we also considered the second lowest value of the mean albedo observed between August and June on Mera Glacier.

Surface albedo of Himalayan glaciers and links with mass balance

F. Brun et al.

Title Page

Abstract

Introduction

Conclusions

References

Tables

Figures

◀

▶

◀

▶

Back

Close

Full Screen / Esc

Printer-friendly Version

Interactive Discussion



This revealed that the second lowest albedo value is often observed more than two months apart from the AMAAG and often exceeds the actual observed minimum by 0.05 to 0.3. In contrast, the second minimum mean albedo measured on Chhota Shigri Glacier is close to the minimum (+0.01) for most years and is generally observed within 10 days. Moreover, the visual inspection of the albedo time series (Fig. 8) confirms a well-defined minimum on Chhota Shigri Glacier, whereas the seasonal cycle of the mean albedo on Mera Glacier is poorly resolved and less marked.

Second, the relation between mass balance and AMAAG is poorly constrained for summer accumulation-type glaciers, where accumulation and ablation occur simultaneously. For Mera Glacier, the range of albedo values used for calibration is narrower than that on Chhota Shigri Glacier (0.47 to 0.55 vs. 0.21 to 0.47). It is also noteworthy that the albedo is calculated from fewer pixels on Mera Glacier than on Chhota Shigri Glacier (16 and 89, respectively), and so the mean albedo obtained for Mera Glacier has a higher uncertainty (Fig. 9b). The AMAAG- B_a relation is also calibrated over a shorter period for Mera Glacier than for Chhota Shigri Glacier (6 years vs. 11). Therefore the regression parameters are less constrained on Mera Glacier than on Chhota Shigri Glacier (Fig. 11), which leads to higher uncertainty.

The choice of the glacier mask is also of major importance for the overall results of our approach. It requires accurate mapping of the glaciers and field experience to eliminate debris-cover zones, rocky area, irregular surfaces (crevasses, seracs) and shaded valleys. In addition, some pixels contain more information about the snowline than others. For instance on Mera Glacier the upper pixels were too affected by the snowfalls and the minimum albedo averaged inside a mask including these pixels did not correlate well with the annual mass balance. Moreover, for Mera Glacier the mask includes only pixels located below the ELA_0 . As a result, the calculated AMAAG should not contain snowline information when the annual mass balance is negative (and ELA is higher than ELA_0). Nevertheless the correlation between B_a and AMAAG holds also for negative mass balance values.

series of ground-based mass balance data with sufficient length are still required to construct robust regression models. Spatial extrapolation of these results to climatologically similar regions and validation with geodetic mass balance estimates would provide a better indication of the transferability of our results, and provide important information on the inter-annual variability glacier mass balance in unmonitored regions of the Hindu Kush-Himalayas.

Acknowledgements. This work has been supported by the French Service d'Observation GLACIOCLIM, the French National Research Agency (ANR) through ANR-PAPRIKA, ANR-PRESHINE, and the French National Space Center (CNES) through TOSCA and ISIS projects, and has been supported by a grant from Labex OSUG@2020 (Investissements d'avenir – ANR10 LABX56). LTHE, CNRM-GAME/CEN and LGGE are part of LabEx OSUG@2020. This study was carried out within the framework of the Ev-K2-CNR Project in collaboration with the Nepal Academy of Science and Technology as foreseen by the Memorandum of Understanding between Nepal and Italy, and thanks to contributions from the Italian National Research Council, the Italian Ministry of Education, University and Research and the Italian Ministry of Foreign Affairs. This work has been conducted in ICIMOD and LTHE, which are greatly acknowledged for their support. JMS is supported by the Cryosphere Monitoring Project, which is funded by the Norwegian Ministry of Foreign Affairs through the Norwegian Embassy in Kathmandu.

References

- Azam, M. F., Wagnon, P., Ramanathan, A., Vincent, C., Sharma, P., Arnaud, Y., Linda, A., Pottakkal, J. G., Chevallier, P., Singh, V. B., and Berthier, E.: From balance to imbalance: a shift in the dynamic behaviour of Chhota Shigri glacier, western Himalaya, India, *J. Glaciol.*, 58, 315–324, doi:10.3189/2012JoG11J123, 2012. 3439, 3441, 3443
- Azam, M. F., Wagnon, P., Vincent, C., Ramanathan, A., Linda, A., and Singh, V. B.: Reconstruction of the annual mass balance of Chhota Shigri glacier, Western Himalaya, India, since 1969, *Ann. Glaciol.*, 55, 69–80, doi:10.3189/2014AoG66A104, 2014a. 3442, 3451, 3473
- Azam, M. F., Wagnon, P., Vincent, C., Ramanathan, A. L., Mandal, A., and Pottakkal, J. G.: Processes governing the mass balance of Chhota Shigri Glacier (Western Himalaya, India)

Surface albedo of Himalayan glaciers and links with mass balance

F. Brun et al.

Title Page

Abstract

Introduction

Conclusions

References

Tables

Figures

◀

▶

◀

▶

Back

Close

Full Screen / Esc

Printer-friendly Version

Interactive Discussion



Surface albedo of Himalayan glaciers and links with mass balance

F. Brun et al.

[Title Page](#)[Abstract](#)[Introduction](#)[Conclusions](#)[References](#)[Tables](#)[Figures](#)[Back](#)[Close](#)[Full Screen / Esc](#)[Printer-friendly Version](#)[Interactive Discussion](#)

assessed by point-scale surface energy balance measurements, *The Cryosphere Discuss.*, 8, 2867–2922, doi:10.5194/tcd-8-2867-2014, 2014b. 3441, 3442, 3443

Berthier, E., Arnaud, Y., Kumar, R., Ahmad, S., Wagnon, P., and Chevallier, P.: Remote sensing estimates of glacier mass balances in the Himachal Pradesh (Western Himalaya, India), *Remote Sens. Environ.*, 108, 327–338, doi:10.1016/j.rse.2006.11.017, 2007. 3439

Bolch, T., Pieczonka, T., and Benn, D. I.: Multi-decadal mass loss of glaciers in the Everest area (Nepal Himalaya) derived from stereo imagery, *The Cryosphere*, 5, 349–358, doi:10.5194/tc-5-349-2011, 2011. 3440

Bolch, T., Kulkarni, A., Kääb, A., Huggel, C., Paul, F., Cogley, J., Frey, H., Kargel, J., Fujita, K., Scheel, M., Bajracharya, S., and Stoffel, M.: The state and fate of Himalayan glaciers, *Science*, 336, 310–314, doi:10.1126/science.1215828, 2012. 3439

Bookhagen, B. and Burbank, D. W.: Topography, relief, and TRMM-derived rainfall variations along the Himalaya, *Geophys. Res. Lett.*, 33, L08405, doi:10.1029/2006GL026037, 2006. 3442

Bookhagen, B. and Burbank, D. W.: Toward a complete Himalayan hydrological budget: spatiotemporal distribution of snowmelt and rainfall and their impact on river discharge, *J. Geophys. Res.-Earth*, 115, F03019, doi:10.1029/2009JF001426, 2010. 3442

Burbank, D. W., Bookhagen, B., Gabet, E. J., and Putkonen, J.: Modern climate and erosion in the Himalaya, *CR Geosci.*, 314, 610–626, doi:10.1016/j.crte.2012.10.010, 2012. 3442

Dumont, M., Sirguey, P., Arnaud, Y., and Six, D.: Monitoring spatial and temporal variations of surface albedo on Saint Sorlin Glacier (French Alps) using terrestrial photography, *The Cryosphere*, 5, 759–771, doi:10.5194/tc-5-759-2011, 2011. 3445

Dumont, M., Gardelle, J., Sirguey, P., Guillot, A., Six, D., Rabatel, A., and Arnaud, Y.: Linking glacier annual mass balance and glacier albedo retrieved from MODIS data, *The Cryosphere*, 6, 1527–1539, doi:10.5194/tc-6-1527-2012, 2012. 3439, 3440, 3445, 3449

Gardelle, J., Berthier, E., Arnaud, Y., and Kääb, A.: Region-wide glacier mass balances over the Pamir-Karakoram-Himalaya during 1999–2011, *The Cryosphere*, 7, 1263–1286, doi:10.5194/tc-7-1263-2013, 2013. 3439, 3440, 3451, 3452, 3473

Gardner, A. S. and Sharp, M. J.: A review of snow and ice albedo and the development of a new physically based broadband albedo parameterization, *J. Geophys. Res.-Earth*, 115, F01009, doi:10.1029/2009JF001444, 2010. 3443

Gardner, A. S., Moholdt, G., Cogley, J. G., Wouters, B., Arendt, A. A., Wahr, J., Berthier, E., Hock, R., Pfeffer, W. T., Kaser, G., Ligtenberg, S. R. M., Bolch, T., Sharp, M. J., Hagen, J. O.,

Surface albedo of Himalayan glaciers and links with mass balance

F. Brun et al.

Title Page

Abstract

Introduction

Conclusions

References

Tables

Figures



Back

Close

Full Screen / Esc

Printer-friendly Version

Interactive Discussion



- van den Broeke, M. R., and Paul, F.: A reconciled estimate of glacier contributions to sea level rise: 2003 to 2009, *Science*, 340, 852–857, doi:10.1126/science.1234532, 2013. 3439
- Garnier, B. and Ohmura, A.: A method of calculating the direct shortwave radiation income of slopes, *J. Appl. Meteorol.*, 7, 796–800, 1968. 3443
- 5 Hall, D. K. and Riggs, G. A.: Accuracy assessment of the MODIS snow products, *Hydrol. Process.*, 21, 1534–1547, doi:10.1002/hyp.6715, 2007. 3453
- Hall, D. K., Riggs, G. A., and Salomonson, V. V.: MODIS/Terra Snow Cover Daily L3 Global 500 m Grid V005, 2000–2013, National Snow and Ice Data Center, Digital media, Boulder, Colorado, USA, 2006 (updated daily). 3444
- 10 Hatwar, H., Yadav, B., Ramarao, Y., and Parikh, R.: Prediction of western disturbances and associated weather over western Himalayas, *Curr. Sci. India*, 88, 913–920, 2005. 3442
- Immerzeel, W., Pellicciotti, F., and Bierkens, M.: Rising river flows throughout the twenty-first century in two Himalayan glacierized watersheds, *Nat. Geosci.*, 6, 742–745, doi:10.1038/NGEO1896, 2013. 3439
- 15 Immerzeel, W. W., van Beek, L. P., and Bierkens, M. F.: Climate change will affect the Asian water towers, *Science*, 328, 1382–1385, doi:10.1126/science.1183188, 2010. 3439
- Kääb, A., Berthier, E., Nuth, C., Gardelle, J., and Arnaud, Y.: Contrasting patterns of early twenty-first-century glacier mass change in the Himalayas, *Nature*, 488, 495–498, doi:10.1038/nature11324, 2012. 3439, 3440
- 20 Kaser, G., Großhauser, M., and Marzeion, B.: Contribution potential of glaciers to water availability in different climate regimes, *P. Natl. Acad. Sci. USA*, 107, 20223–20227, doi:10.1073/pnas.1008162107, 2010. 3439
- Klein, A. G. and Stroeve, J.: Development and validation of a snow albedo algorithm for the MODIS instrument, *Ann. Glaciol.*, 34, 45–52, 2002. 3444
- 25 Maussion, F., Scherer, D., Mölg, T., Collier, E., Curio, J., and Finkelnburg, R.: Precipitation seasonality and variability over the Tibetan Plateau as resolved by the High Asia Reanalysis, *J. Climate*, 27, 1910–1927, doi:10.1175/JCLI-D-13-00282.1, 2013. 3442
- Ming, J., Du, Z., Xiao, C., Xu, X., and Zhang, D.: Darkening of the mid-Himalaya glaciers since 2000 and the potential causes, *Environ. Res. Lett.*, 7, 014021, doi:10.1088/1748-9326/7/1/014021, 2012. 3448, 3453, 3455
- 30 Nuimura, T., Fujita, K., Yamaguchi, S., and Sharma, R. R.: Elevation changes of glaciers revealed by multitemporal digital elevation models calibrated by GPS survey in the Khumbu

Surface albedo of Himalayan glaciers and links with mass balance

F. Brun et al.

Title Page

Abstract

Introduction

Conclusions

References

Tables

Figures

◀

▶

◀

▶

Back

Close

Full Screen / Esc

Printer-friendly Version

Interactive Discussion



region, Nepal Himalaya, 1992–2008, *J. Glaciol.*, 58, 648–656, doi:10.3189/2012JoG11J061, 2012. 3439, 3440

Rabatel, A., Dedieu, J.-P., and Vincent, C.: Using remote-sensing data to determine equilibrium-line altitude and mass-balance time series: validation on three French glaciers, 1994–2002, *J. Glaciol.*, 51, 539–546, 2005. 3440, 3449

Rabatel, A., Letréguilly, A., Dedieu, J.-P., and Eckert, N.: Changes in glacier equilibrium-line altitude in the western Alps from 1984 to 2010: evaluation by remote sensing and modeling of the morpho-topographic and climate controls, *The Cryosphere*, 7, 1455–1471, doi:10.5194/tc-7-1455-2013, 2013. 3440

Radić, V., Bliss, A., Beedlow, A., Hock, R., Miles, E., and Cogley, J.: Regional and global projections of twenty-first century glacier mass changes in response to climate scenarios from global climate models, *Clim. Dynam.*, 42, 37–58, doi:10.1007/s00382-013-1719-7, 2014. 3439

Richardson, S. D. and Reynolds, J. M.: An overview of glacial hazards in the Himalayas, *Quatern. Int.*, 65, 31–47, 2000. 3439

Shea, J. M., Menounos, B., Moore, R. D., and Tennant, C.: An approach to derive regional snow lines and glacier mass change from MODIS imagery, western North America, *The Cryosphere*, 7, 667–680, doi:10.5194/tc-7-667-2013, 2013. 3440

Shrestha, D., Singh, P., and Nakamura, K.: Spatiotemporal variation of rainfall over the central Himalayan region revealed by TRMM Precipitation Radar, *J. Geophys. Res.-Atmos.*, 117, D22106, doi:10.1029/2012JD018140, 2012. 3442

Sirguey, P.: Simple correction of multiple reflection effects in rugged terrain, *Int. J. Remote Sens.*, 30, 1075–1081, doi:10.1080/01431160802348101, 2009. 3445

Sirguey, P., Mathieu, R., and Arnaud, Y.: Subpixel monitoring of the seasonal snow cover with MODIS at 250m spatial resolution in the Southern Alps of New Zealand: Methodology and accuracy assessment, *Remote Sens. Environ.*, 113, 160–181, doi:10.1016/j.rse.2008.09.008, 2009. 3445, 3453

Şorman, A. Ü., Akyürek, Z., Şensoy, A., Şorman, A. A., and Tekeli, A. E.: Commentary on comparison of MODIS snow cover and albedo products with ground observations over the mountainous terrain of Turkey, *Hydrol. Earth Syst. Sci.*, 11, 1353–1360, doi:10.5194/hess-11-1353-2007, 2007. 3447

Surface albedo of Himalayan glaciers and links with mass balance

F. Brun et al.

Title Page

Abstract

Introduction

Conclusions

References

Tables

Figures

◀

▶

◀

▶

Back

Close

Full Screen / Esc

Printer-friendly Version

Interactive Discussion



Thibert, E., Blanc, R., Vincent, C., and Eckert, N.: Instruments and Methods Glaciological and volumetric mass-balance measurements: error analysis over 51 years for Glacier de Sarennes, French Alps, *J. Glaciol.*, 54, 522–532, 2008. 3443

Vincent, C., Ramanathan, A., Wagnon, P., Dobhal, D. P., Linda, A., Berthier, E., Sharma, P., Arnaud, Y., Azam, M. F., Jose, P. G., and Gardelle, J.: Balanced conditions or slight mass gain of glaciers in the Lahaul and Spiti region (northern India, Himalaya) during the nineties preceded recent mass loss, *The Cryosphere*, 7, 569–582, doi:10.5194/tc-7-569-2013, 2013. 3439, 3440, 3441

Wagnon, P., Linda, A., Arnaud, Y., Kumar, R., Sharma, P., Vincent, C., Pottakkal, J. G., Berthier, E., Ramanathan, A., Hasnain, S. I., and Chevallier, P.: Four years of mass balance on Chhota Shigri Glacier, Himachal Pradesh, India, a new benchmark glacier in the western Himalaya, *J. Glaciol.*, 53, 603–611, 2007. 3441, 3442, 3445

Wagnon, P., Vincent, C., Arnaud, Y., Berthier, E., Vuillemoz, E., Gruber, S., Ménégoz, M., Gilbert, A., Dumont, M., Shea, J. M., Stumm, D., and Pokhrel, B. K.: Seasonal and annual mass balances of Mera and Pokalde glaciers (Nepal Himalaya) since 2007, *The Cryosphere*, 7, 1769–1786, doi:10.5194/tc-7-1769-2013, 2013. 3439, 3441, 3442, 3443, 3445, 3450

Warren, S. G.: Optical properties of snow, *Rev. Geophys.*, 20, 67–89, doi:10.1029/RG020i001p00067, 1982. 3443, 3444

Yao, T., Thompson, L., Yang, W., Yu, W., Gao, Y., Guo, X., Yang, X., Duan, K., Zhao, H., Xu, B., Pu, J., Lu, A., Xiang, Y., Kattel, D. B., and Joswiak, D.: Different glacier status with atmospheric circulations in Tibetan Plateau and surroundings, *Nature Climate Change*, 2, 663–667, doi:10.1038/NCLIMATE1580, 2012. 3442

Zemp, M., Thibert, E., Huss, M., Stumm, D., Rolstad Denby, C., Nuth, C., Nussbaumer, S. U., Moholdt, G., Mercer, A., Mayer, C., Joerg, P. C., Jansson, P., Hynek, B., Fischer, A., Escher-Vetter, H., Elvehøy, H., and Andreassen, L. M.: Reanalysing glacier mass balance measurement series, *The Cryosphere*, 7, 1227–1245, doi:10.5194/tc-7-1227-2013, 2013. 3451

Zhang, J. and Reid, J. S.: A decadal regional and global trend analysis of the aerosol optical depth using a data-assimilation grade over-water MODIS and Level 2 MISR aerosol products, *Atmos. Chem. Phys.*, 10, 10949–10963, doi:10.5194/acp-10-10949-2010, 2010. 3453

Surface albedo of Himalayan glaciers and links with mass balance

F. Brun et al.

Title Page

Abstract

Introduction

Conclusions

References

Tables

Figures

◀

▶

◀

▶

Back

Close

Full Screen / Esc

Printer-friendly Version

Interactive Discussion



Table 1. MODImLab inputs.

Data name	Description	Availability
MOD02QKM	TOA radiances for bands 1 and 2; 250 m resolution	ladsweb.nascom.nasa.gov
MOD02HKM	TOA radiances for bands 3 to 7; 500 m resolution	ladsweb.nascom.nasa.gov
MOD021KM	TOA radiances for bands 8 to 36; 1 km resolution	ladsweb.nascom.nasa.gov
MOD03 GDEM	Geolocation; 1 km resolution ASTER DEM at ~ 30 m resolution resampled at 125 m resolution	ladsweb.nascom.nasa.gov asterweb.jpl.nasa.gov
Aeronet AOD	AOD measured at Ev-K2-CNR-Pyramid; data available from Apr 2006 to May 2011	aeronet.gsfc.nasa.gov
OMI	Total ozone column; data available from Jul 2004; 1° resolution	ozoneaq.gsfc.nasa.gov

Surface albedo of Himalayan glaciers and links with mass balance

F. Brun et al.

Table 2. Values of the observed minima of the mean albedo and dates at which they are observed. At Mera Glacier, minimum albedo dates can occur between 1 August and 30 June of the following year. The data used for the calibration are in bold.

Year	Chhota Shigri		Mera	
99–00	4 Sep 2000	0.263	10 Feb 2001	0.553
00–01	27 Aug 2001	0.217	18 Apr 2002	0.660
01–02	9 Aug 2002	0.243	27 Mar 2003	0.593
02–03	25 Jul 2003	0.219	29 Mar 2004	0.498
03–04	13 Sep 2004	0.246	23 May 2005	0.509
04–05	22 Aug 2005	0.318	30 Jan 2006	0.395
05–06	18 Aug 2006	0.236	3 Jul 2007	0.442
06–07	30 Aug 2007	0.287	9 Apr 2008	0.730
07–08	7 Aug 2008	0.237	2 Mar 2009	0.514
08–09	25 Aug 2009	0.356	6 Apr 2010	0.501
09–10	3 Aug 2010	0.446	27 May 2011	0.469
10–11	12 Sep 2011	0.468	10 Aug 2011	0.545
11–12	12 Sep 2012	0.286	1 Jan 2013	0.474
12–13	25 Aug 2013	0.270	7 Oct 2013	0.485

Title Page

Abstract

Introduction

Conclusions

References

Tables

Figures

◀

▶

◀

▶

Back

Close

Full Screen / Esc

Printer-friendly Version

Interactive Discussion



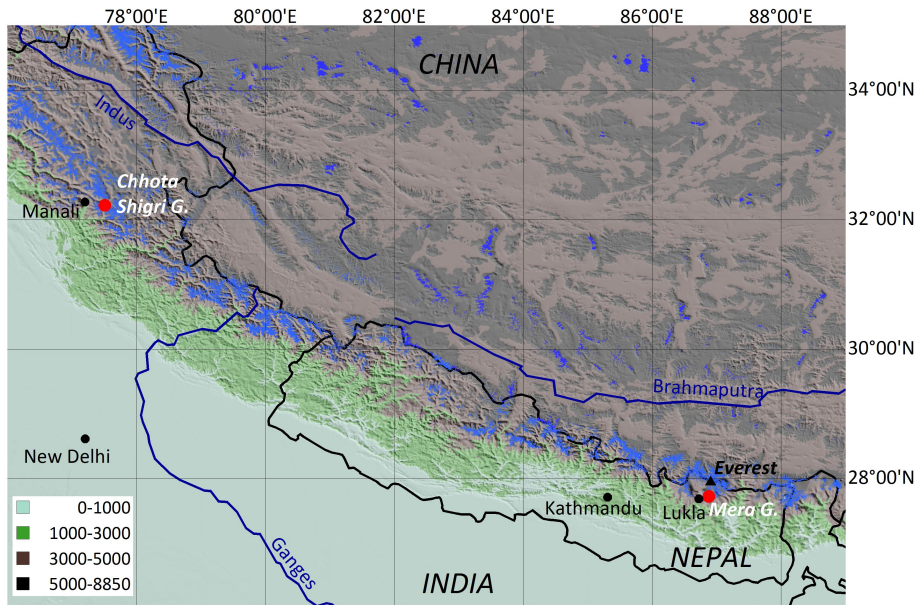


Figure 1. Map of the study area. The altitude ranges given in the legend are in meters. The glacierized areas are in blue and the two studied glaciers are represented by red dots.

Surface albedo of Himalayan glaciers and links with mass balance

F. Brun et al.

Title Page

Abstract

Introduction

Conclusions

References

Tables

Figures

◀

▶

◀

▶

Back

Close

Full Screen / Esc

Printer-friendly Version

Interactive Discussion



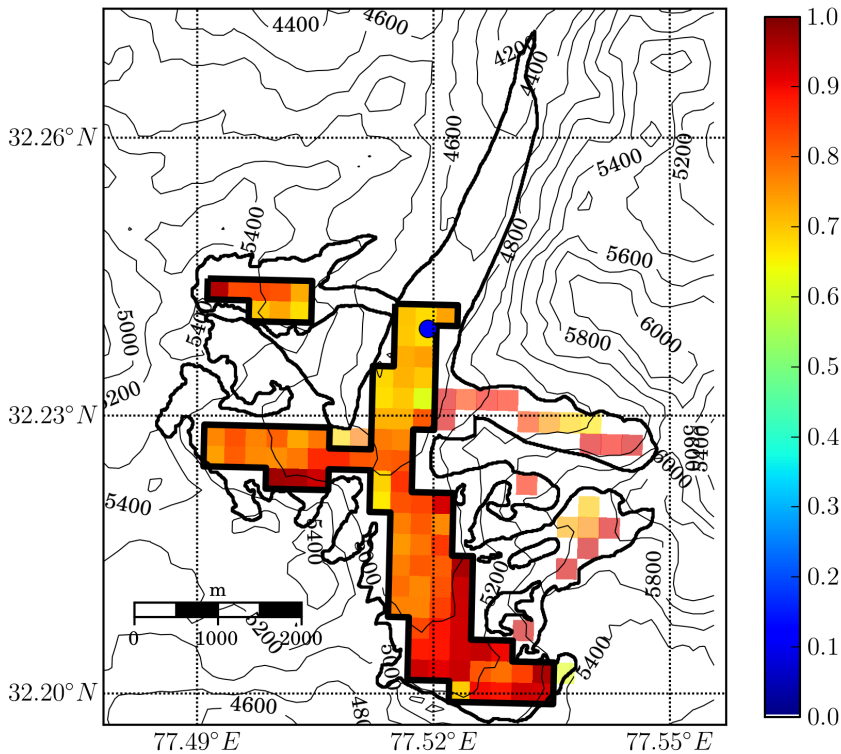


Figure 2. Example of an albedo map retrieved by MODImLab over Chhota Shigri Glacier on 5 October 2004 05:20:00 (UTC). The bold line delimits the pixels used to average the albedo ($n = 89$, corresponding to 4.875 km^2). The northern lower part of the glacier is covered with debris and the tributaries exhibit surfaces that include many rock outcrops. The blue dot shows the location of the AWS.

Surface albedo of Himalayan glaciers and links with mass balance

F. Brun et al.

Title Page	
Abstract	Introduction
Conclusions	References
Tables	Figures
◀	▶
◀	▶
Back	Close
Full Screen / Esc	
Printer-friendly Version	
Interactive Discussion	



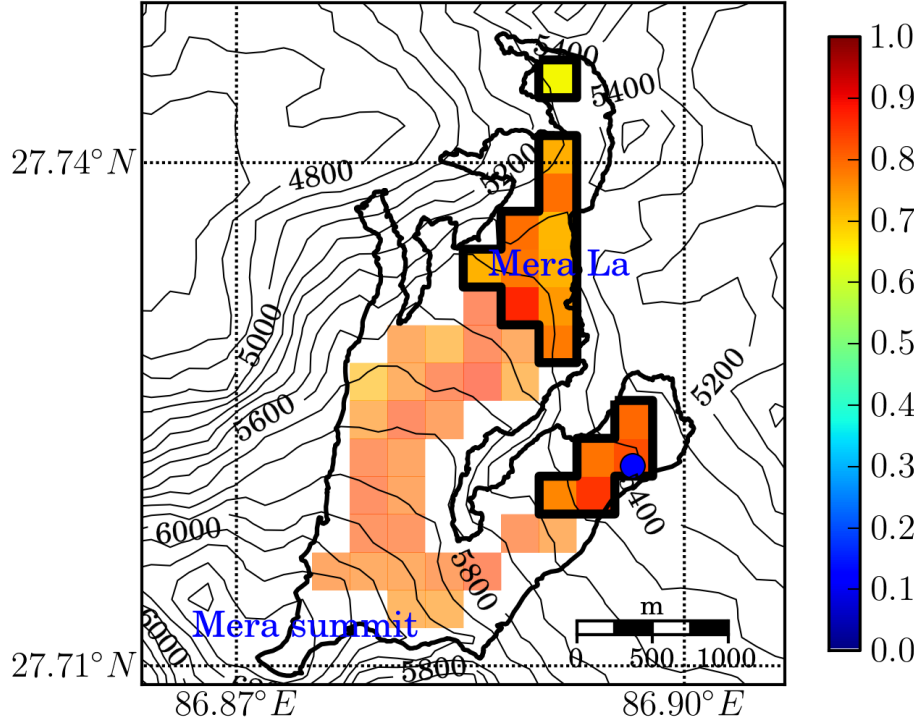


Figure 3. Example of an albedo map retrieved by MODImLab over Mera Glacier on 6 October 2006 05:00:00 (UTC). The bold line delimits the pixels used to average the albedo ($n = 16$, corresponding to 1 km^2) which are located below 5550 m a.s.l. The blue dot shows the location of the AWS.

Surface albedo of Himalayan glaciers and links with mass balance

F. Brun et al.

Title Page	
Abstract	Introduction
Conclusions	References
Tables	Figures
◀	▶
◀	▶
Back	Close
Full Screen / Esc	
Printer-friendly Version	
Interactive Discussion	



Surface albedo of Himalayan glaciers and links with mass balance

F. Brun et al.

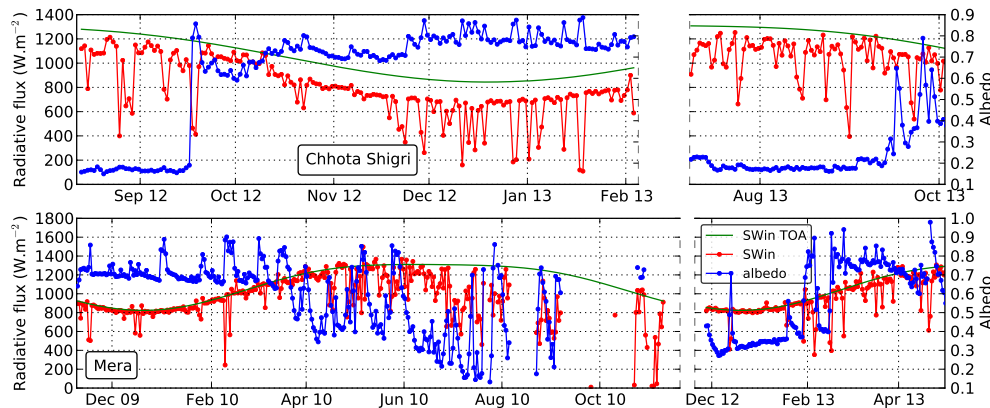


Figure 4. Measured (red) and modelled top of the atmosphere (green) incoming shortwave radiation and albedo (blue) for Chhota Shigri (top) and Mera (bottom) glaciers. The values reported are the daily maxima of the radiative flux. The daily albedo is calculated as the average of the albedo on a two-hour time span centered on the satellite passing time.

[Title Page](#)[Abstract](#)[Introduction](#)[Conclusions](#)[References](#)[Tables](#)[Figures](#)[◀](#)[▶](#)[◀](#)[▶](#)[Back](#)[Close](#)[Full Screen / Esc](#)[Printer-friendly Version](#)[Interactive Discussion](#)

Surface albedo of Himalayan glaciers and links with mass balance

F. Brun et al.

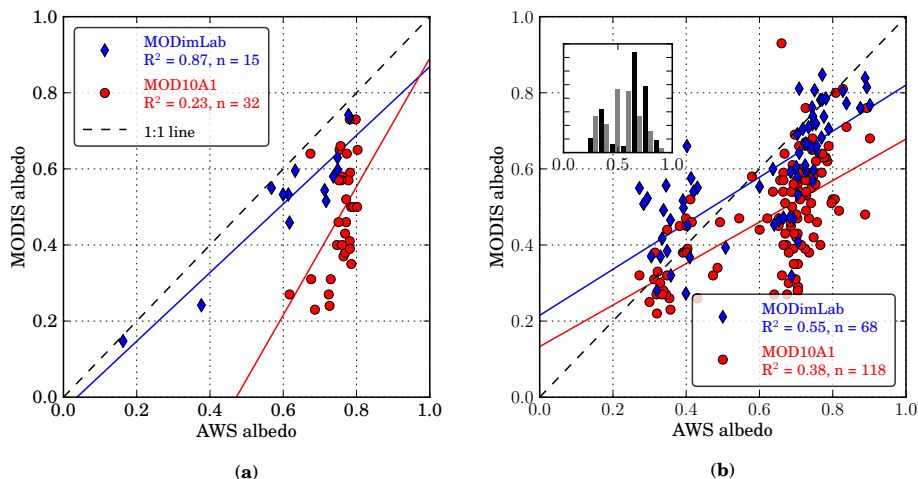


Figure 5. Measured albedo vs. MODIS retrieved albedo for Chhota Shigri Glacier **(a)** and Mera Glacier **(b)**. For Mera Glacier RMSE are 0.067 and 0.071 for the MODImLab and the MOD10, respectively. The inset represents the distribution of the measured albedo (grey = satellite, black = AWS).

Discussion Paper | Discussion Paper | Discussion Paper | Discussion Paper | Discussion Paper

Title Page

Abstract Introduction

Conclusions References

Tables Figures

◀ ▶

◀ ▶

Back Close

Full Screen / Esc

Printer-friendly Version

Interactive Discussion



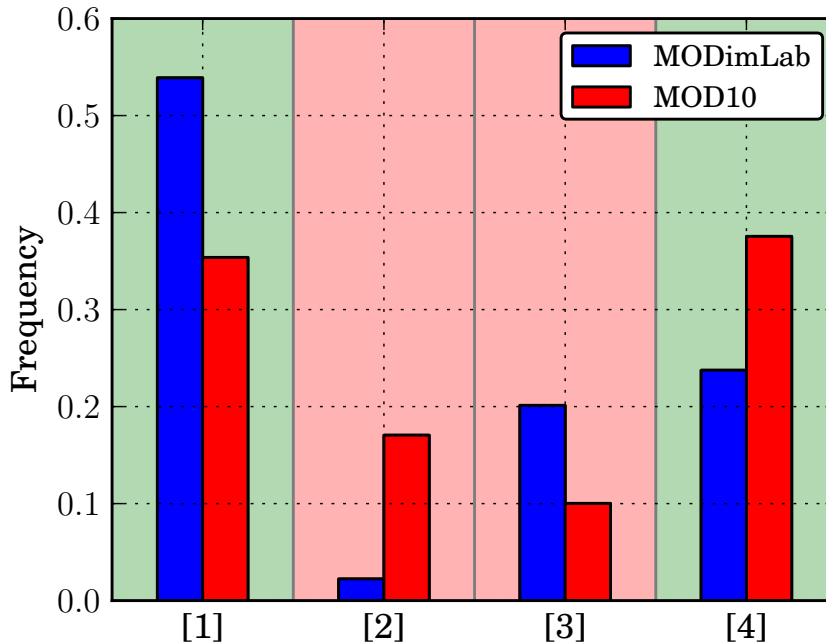


Figure 6. Frequency of occurrences of hit rate and confusions in the classification of clouds by MODImLab ($n = 13312$ pixels) and MOD10 ($n = 3328$ pixels). Reference data were obtained via visual interpretation of clouds in simultaneous ASTER images. Category 1 corresponds to cloudy pixels detected as cloudy pixels, category 2 to cloudy pixels detected as cloud-free pixels, category 3 to cloud-free pixels detected as cloudy pixels and category 4 to cloud-free pixels detected as cloud-free pixels. Categories 1 and 4 correspond to the correctly classified pixels (green background) and categories 2 and 3 correspond to the misclassified pixels (red background).

Surface albedo of Himalayan glaciers and links with mass balance

F. Brun et al.

Title Page

Abstract Introduction

Conclusions References

Tables Figures

◀ ▶

◀ ▶

Back Close

Full Screen / Esc

Printer-friendly Version

Interactive Discussion



Surface albedo of Himalayan glaciers and links with mass balance

F. Brun et al.

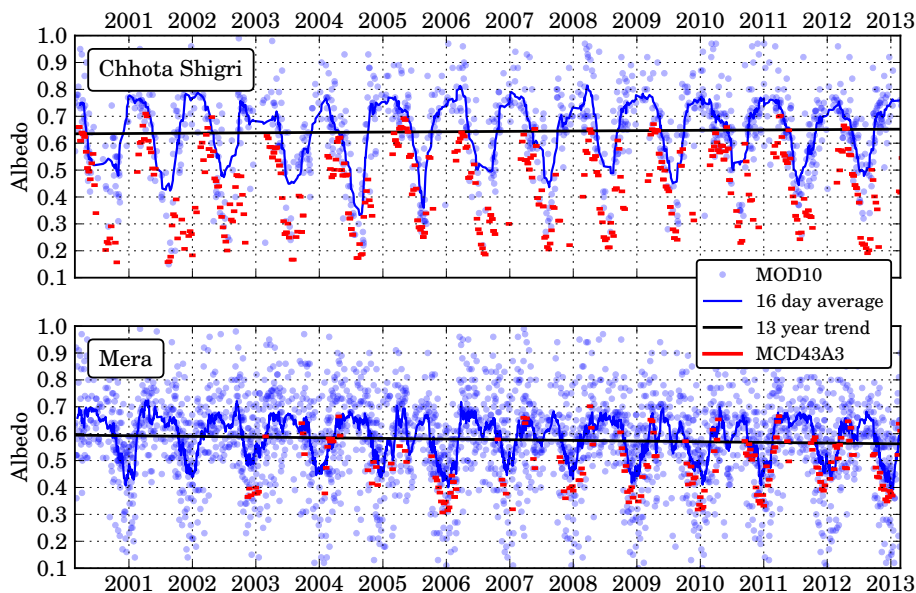


Figure 7. MOD10 daily albedo (cyan dots) and 10 day running average (solid blue line) for the highest pixel of Chhota Shigri Glacier (upper panel; pixel at 5191 m a.s.l.) and Mera Glacier (lower panel; pixel at 6008 m a.s.l.). The solid black line represents the 13 year linear trend in albedo ($+0.0013 \text{ yr}^{-1}$ for Chhota Shigri Glacier and -0.0025 yr^{-1} for Mera Glacier). The red dots are the MCD43 8 day albedo constructed from multiangle acquisitions over 16 days. Only 22% of MCD43 data-points correspond to good quality products on Chhota Shigri Glacier and only 4% on Mera Glacier.

Title Page

Abstract

Introduction

Conclusions

References

Tables

Figures

◀

▶

◀

▶

Back

Close

Full Screen / Esc

Printer-friendly Version

Interactive Discussion



Surface albedo of Himalayan glaciers and links with mass balance

F. Brun et al.

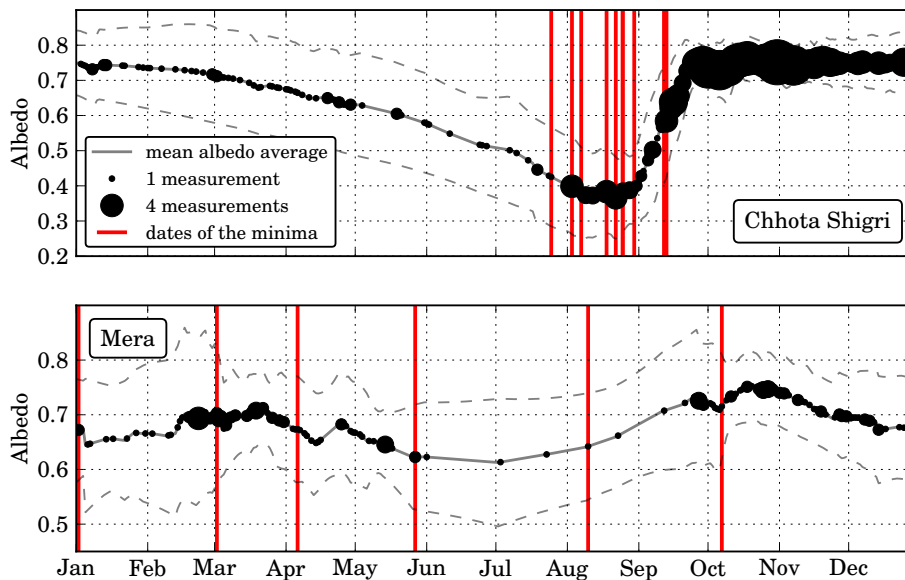


Figure 8. Seasonal variations of the mean albedo for Chhota Shigri (top) and Mera (bottom) glaciers. The solid grey line represents the average of the interpolated daily mean albedo with a $1\text{-}\sigma$ envelope (dashed grey lines). Note that the scaling of albedo is different on both panels. The size of dots is proportional to the number of good quality images available for the Julian day. The vertical red bars indicate the dates of annual minima for each year under consideration.

[Title Page](#)[Abstract](#)[Introduction](#)[Conclusions](#)[References](#)[Tables](#)[Figures](#)[◀](#)[▶](#)[◀](#)[▶](#)[Back](#)[Close](#)[Full Screen / Esc](#)[Printer-friendly Version](#)[Interactive Discussion](#)

Surface albedo of Himalayan glaciers and links with mass balance

F. Brun et al.

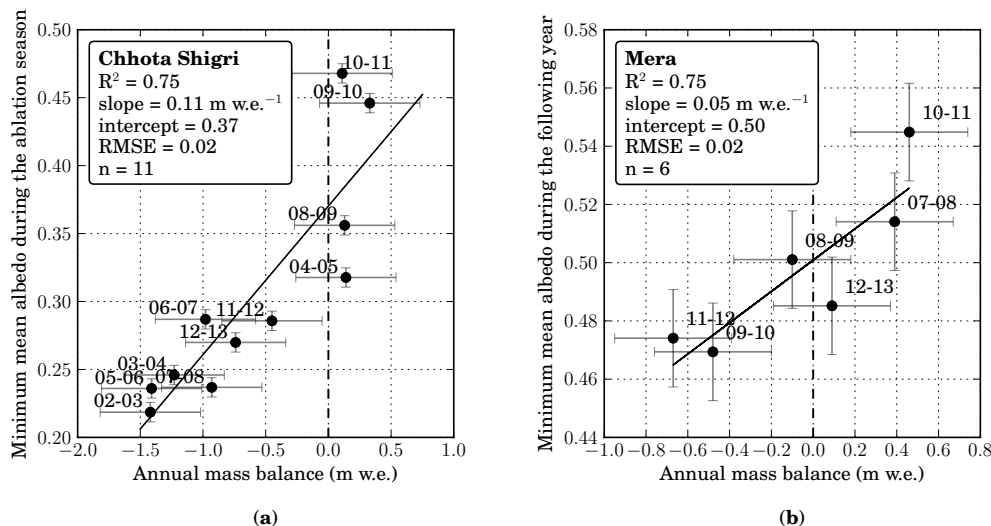


Figure 9. AMAAG as a function of B_a for Chhota Shigri Glacier (a) and Mera Glacier (b). The error bars for the mass balance are $\pm 0.40 \text{ m.w.e.}$ and $\pm 0.28 \text{ m.w.e.}$ for Chhota Shigri and Mera glaciers, respectively. The uncertainty on the mean albedo is calculated as the accuracy of the MODImLab albedo established on Mera Glacier (RMSE = 0.067) divided by the root mean square of the number of pixels in the average ($n = 89$ and $n = 16$ for Chhota Shigri and Mera glaciers, respectively). At Mera Glacier, the 2012–2013 mass balance has been calculated excluding the heavy snow fall that occurred 13–15 October 2013 to be consistent with the end of the hydrological year ending with the ablation season. It is noteworthy that this mass balance also has a larger uncertainty (not shown on the figure) because of ablation measurements were partly compromised by stakes buried in the snow.

Title Page

Abstract Introduction

Conclusions References

Tables Figures

◀ ▶

◀ ▶

Back Close

Full Screen / Esc

Printer-friendly Version

Interactive Discussion



Surface albedo of Himalayan glaciers and links with mass balance

F. Brun et al.

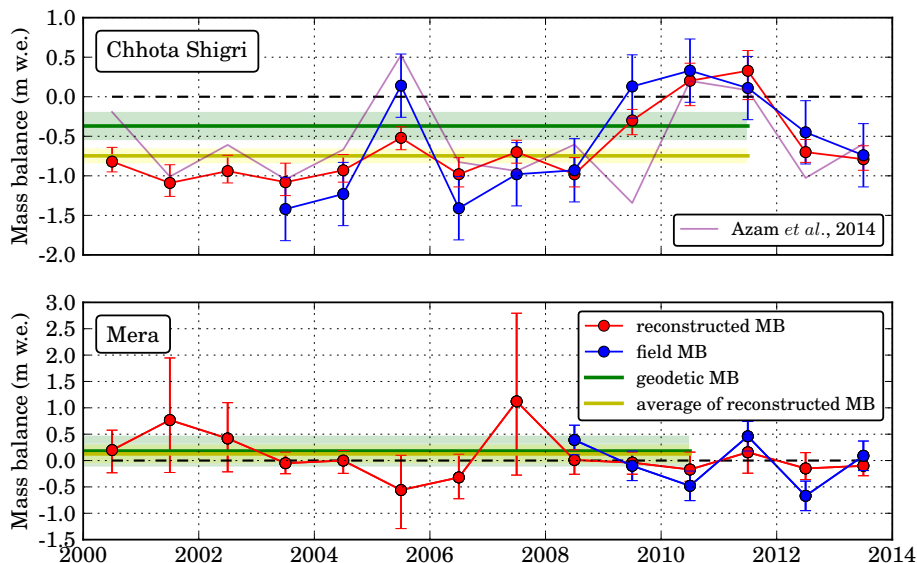


Figure 10. Reconstructed mass balance for Chhota Shigri (top) and Mera (bottom) glaciers. The green and yellow lines represent the annual mean of the geodetic mass balance from Gardelle et al. (2013) and the annual mean of the reconstructed mass balance, respectively. The purple line corresponds to the annual mass balance values calculated with a degree-day model (Azam et al., 2014a). The error bars for the reconstructed mass balance correspond to the 90 % confidence interval. For Mera Glacier some reconstructed mass balance values (for the years 2001 and 2007) correspond to albedo values outside the range of calibration and are therefore believed to be questionable. Note that the scaling of mass balance is different on both panels.

Title Page

Abstract

Introduction

Conclusions

References

Tables

Figures

◀

▶

◀

▶

Back

Close

Full Screen / Esc

Printer-friendly Version

Interactive Discussion



Surface albedo of Himalayan glaciers and links with mass balance

F. Brun et al.

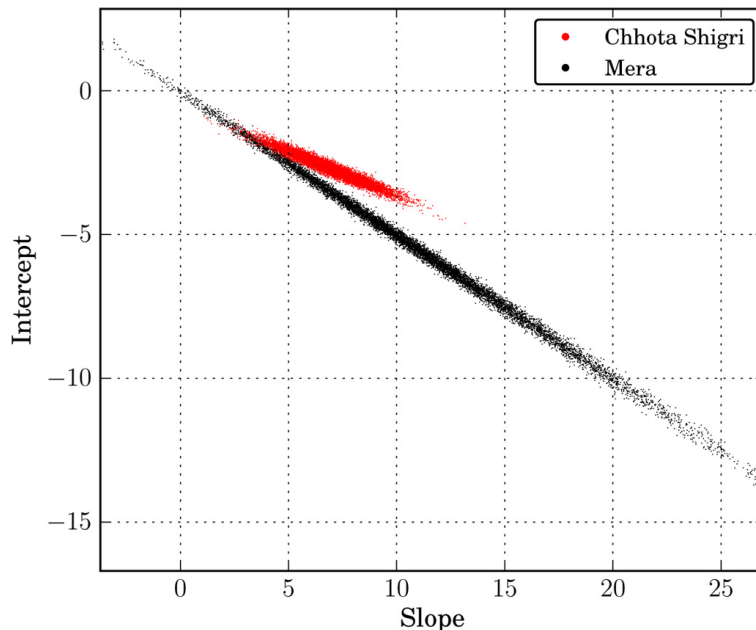


Figure 11. Regression parameters obtained from the Monte Carlo simulation ($N = 10000$). Every data-point represents a slope-intercept couple obtained as the best fit of B_a as a function of AMAAG.

[Title Page](#)[Abstract](#)[Introduction](#)[Conclusions](#)[References](#)[Tables](#)[Figures](#)[◀](#)[▶](#)[◀](#)[▶](#)[Back](#)[Close](#)[Full Screen / Esc](#)[Printer-friendly Version](#)[Interactive Discussion](#)